Crucial role of interfacial alloying on spin-transfer torque in magnetic tunnel junctions

Y.-H. Tang and Nicholas Kioussis

Phys. Rev. B **85**, 104413 — Published 22 March 2012

DOI: 10.1103/PhysRevB.85.104413

Crucial Role of Interfacial Alloying on Spin Transfer Torque in Magnetic Tunnel Junctions

Y. -H. Tang[1] and Nicholas Kioussis[2]

[1]*Department of Physics, National Central University, Jung-Li 32001, Taiwan**
[2]*Department of Physics, California State University, Northridge, CA 91330-8268, USA*†

(Dated: March 7, 2012)

We demonstrate that interfacial disorder in magnetic tunnel junctions (MTJs) has a dramatic effect on the bias behavior of both spin-transfer and field-like spin torques, leading to strong enhancement, sign reversal, and bias asymmetry. The underlying mechanism lies on the impurity-induced resonance energies which can be selectively controlled with alloying and/or bias. The predictions explain for the first time the experimental results in "dirty" junctions and have important implications on exploiting further the alloying effect to optimize the current induced magnetization switching.

PACS numbers: 85.75.-d, 72.25.-b, 73.40.Gk

I. INTRODUCTION

Magnetic tunnel junctions (MTJs), consisting of two ferromagnetic (FM) metal layers separated by a thin insulating barrier (IB) layer, have attracted wide and sustained interest due to their potential applications in nonvolatile magnetic-random access memories (MRAM) and as magnetic-field sensors in magnetic hard disk drives[1–3]. Because of the limitations (scaling issue, cross talk, heat diffusion, and poor reliability) associated with the external magnetic field in the writing process of MRAM, the recently discovered current-induced magnetization reversal (CIMR)[4–6] via the so-called spin torque effect, originally predicted by Slonczewski[7] and Berger[8], is considered as a promising plausible solution. In ideal symmetric MTJs we have predicted[9,10] an anomalous bias behavior of the spin-transfer torque, $T_\parallel$, which can exhibit a sign reversal without a corresponding sign reversal of the bias or even a quadratic bias dependence. On the other hand, experiments indicate[11–13] that $T_\parallel$ reverses sign on changing the current direction. Furthermore, in asymmetric MTJs we have recently demonstrated[14,15] that the bias behavior of the field-like spin torque, $T_\perp$, can be selectively controlled via the asymmetry in band filling between the FM leads, thus leading to a linear and/or quadratic low-bias behavior in agreement with experiment.[16]

Real Fe/MgO/Fe MTJs almost invariably are "dirty" containing interfacial vacancies or structural defects that, even if only present in a limited density, can dominate both the tunnel magnetoresistance (TMR)[17–23] and the zero-bias interlayer exchange coupling (IEC)[24]. Recently, Ikeda *et al* have reported[25] that the room-temperature TMR in CoFeB/MgO/CoFeB MTJs annealed at 525°C increases to 604%, which approaches the theoretical value[26,27]. This high TMR value has been attributed to the high crystalline quality of the FM leads via the annealing process. X-ray photoelectron spectroscopy[20] and three-dimensional atom probe studies[21] have directly observed the diffusion of B from the electrodes into the MgO layer upon annealing, giving rise to the formation of B oxide, the reduction of the Fe(Co) oxide and a concomitant enhancement in TMR. In contrast, electronic structure calculations[28] have shown that the presence of B at the interface is detrimental to the TMR due to significant suppression of the majority-channel conductance through the Δ_1 state symmetry.

On the theoretical side, using the free-electron model Manchon *et al.*[29] studied the effect of a layer of impurities in the barrier on the bias dependence of $T_\parallel$ and TMR and the effect of the impurity energy level on the zero bias of $T_\perp$. Birol *et al.*[30] calculated the contribution to the spin-transfer torque in a MTJ from sequential tunneling through interacting impurities and determined the angular dependence of spin torques as a function of the spin polarization of the ferromagnetic leads. Recently, employing the tight-binding (TB) model and the Keldysh formalism we have developed[31] a computational approach which allows the study of the effect of disorder in the barrier on the average spin transfer torque. We have also demonstrated that the general expression of the bias behavior of $T_\parallel$ in terms of the interplay of the average spin current densities in collinear configurations [Eq. (1) in Ref.[31]], remains valid even in the presence of non-magnetic impurities. This in turn leads to a sinusoidal angular behavior of $T_\parallel$.

In contrast to the monotonic variation of the density of states (DOS) in the free-electron model employed in Ref.[29], the TB model employed in this work yields non-monotonic DOS. Therefore, the free-electron model is only correct in the low-bias and or low band filling regime [9,29]. In addition, the bias voltage must be smaller than the half bandwidth of the conduction electrons. Consequently, neither the band filling-induced sign reversal of the interlayer exchange coupling nor the oscillatory bias dependence of $T_\perp$ revealed in our TB calculations in Refs. [14,15] can be obtained within the free-electron model. Furthermore, the pure quadratic bias behavior of $T_\parallel$ we predicted[9] is possible within the TB model due to the bell-like form of the density of states [Fig. 1 of Ref.[10]] at the interfaces.

In this study, we apply the computational method

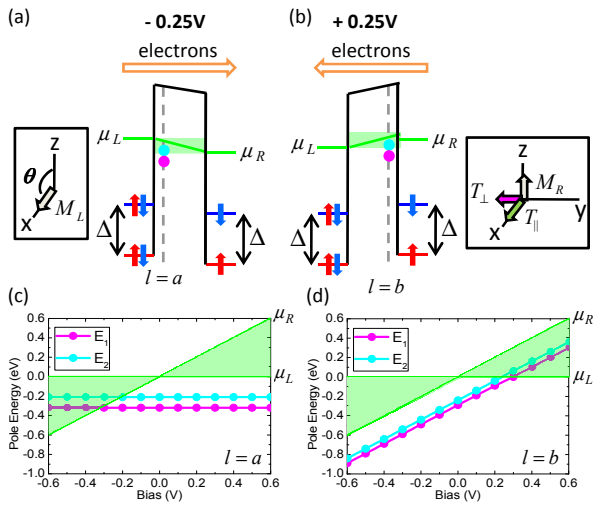

FIG. 1: (Color online) (a) and (b) Schematic of disordered MTJs with a layer of non-magnetic impurities with on-site ε_{imp}= 0.0eV at the first (last) IB layer at the left (right) interface, $l = a$ ($l = b$), under -0.25V (+0.25V) bias. The red and blue horizontal solid lines represent the bottom of the majority- and minority-spin energy bands of the FM leads , respectively, where Δ denotes the exchange energy splitting. The magenta and cyan solid circles denote the impurity-induced resonance energies, E_1 and E_2. The net spin-transfer, $T_\parallel$, and field-like, $T_\perp$, components of spin torque on the right FM lead are along $\hat{M}_R \times (\hat{M}_L \times \hat{M}_R)$ and $\hat{M}_L \times \hat{M}_R$, respectively, where $\hat{M}_{L(R)}$ is the unit vector of the magnetization in the left (right) FM lead. (c) and (d) The bias dependence of E_1 and E_2 for the impurity layers at $l = a$ and $l = b$, respectively. The bias window between the chemical potentials, μ_L and μ_R, of the left and right FM leads, respectively, is denoted by the green shaded area.

which we have recently developed[31], and provide a comprehensive study of the effect of disorder on the bias behavior of both components of the spin transfer torque for symmetric and asymmetric disorder configurations. We demonstrate that non-magnetic interfacial point defects have a dramatic effect on the *average* $\langle T_\perp(V)\rangle$ and $\langle T_\parallel(V)\rangle$, including a strong enhancement, sign reversal, and bias asymmetry. The underlying mechanism lies on the impurity-induced resonance states, which can be selectively controlled with bias and/or gate voltage and impurity position.

II. METHODOLOGY

The calculations are based on the TB method and the non-equilibrium Keldysh formalism. We consider single and double impurity layers (indexed by their lth position) inside the IB with impurity concentration $c \sim 2.7\%$. The non-magnetic impurity scattering potential is of a δ-function form, i.e. $\hat{W} = \Big[\varepsilon_{imp}\delta(i-l) - \varepsilon_b\Big]\hat{I}$, where ε_b and ε_{imp} are the IB and impurity on-site energies, respectively, i refers to an arbitrary layer inside the IB, and $\hat{I}$ is a 2×2 unit matrix. We employ the same set of TB parameters of our previous theoretical predictions[9,15] in ideal symmetric and asymmetric MTJs, which provides a realistic description of systems based on magnetic transition metals and their alloys.

The 2×2 Keldysh Green's function spin matrix, $\hat{\mathbb{G}}^<(\overrightarrow{\rho}, i; \overrightarrow{\rho}', j)$, in the presence of disorder can be expanded [31] in terms of the $\hat{\mathbb{T}}$-matrices of the perturbing impurity scattering potential, $\hat{W}$. Here, i and j denote the coordinates along the transport direction (y-axis in Fig. 1), and $\overrightarrow{\rho}$, and $\overrightarrow{\rho}'$ are two-dimensional vectors within the x-z plane. The 2×2 impurity retarded and advanced scattering $\hat{\mathbb{T}}$-matrices are of the form,

$$\hat{\mathbb{T}}^R = \hat{W}\big[\hat{I} - \hat{W}\hat{G}(\overrightarrow{\rho_0}, l; \overrightarrow{\rho_0}, l)\big]^{-1},$$
$$\hat{\mathbb{T}}^A = \hat{W}\big[\hat{I} - \hat{W}\hat{\tilde{G}}(\overrightarrow{\rho_0}, l; \overrightarrow{\rho_0}, l)\big]^{-1}, \quad (1)$$

respectively. Here, $\hat{G}$ and $\hat{\tilde{G}}$ are the 2×2 retarded and advanced Green's function matrices in the clean MTJs, and $\overrightarrow{\rho_0}$ and l denote the impurity's coordinates parallel and perpendicular to the interface, respectively. The impurity-induced resonant energies correspond to the zeroes of the determinant of the denominators in Eq. (1), which can be written as,

$$\|\hat{I} - \hat{W}\hat{G}(\overrightarrow{\rho_0}, l; \overrightarrow{\rho_0}, l)\| =$$
$$\big[1 - wG^{\uparrow\uparrow}(\overrightarrow{\rho_0}, l; \overrightarrow{\rho_0}, l)\big]\big[1 - wG^{\downarrow\downarrow}(\overrightarrow{\rho_0}, l; \overrightarrow{\rho_0}, l)\big] -$$
$$w^2 G^{\uparrow\downarrow}(\overrightarrow{\rho_0}, l; \overrightarrow{\rho_0}, l)G^{\downarrow\uparrow}(\overrightarrow{\rho_0}, l; \overrightarrow{\rho_0}, l)$$
$$\sim \big[1 - wG^{\uparrow\uparrow}(\overrightarrow{\rho_0}, l; \overrightarrow{\rho_0}, l)\big]\big[1 - wG^{\downarrow\downarrow}(\overrightarrow{\rho_0}, l; \overrightarrow{\rho_0}, l)\big], \quad (2)$$

because $G^{\uparrow\downarrow(\downarrow\uparrow)}(\overrightarrow{\rho_0}, l; \overrightarrow{\rho_0}, l)$ is very small due to the fact that the impurity site l is inside the barrier. Here, $w = (\varepsilon_{imp} - \varepsilon_b)$. The product of the bracket terms in the above equation is quadratic in energy leading to the two poles E_1 and E_2. Note however, if the impurity site l is away from the FM/IB interfaces, then $E_1 \sim E_2$ since $G^{\uparrow\uparrow}_{ll} \approx G^{\downarrow\downarrow}_{ll}$ for non-magnetic IB. Since we consider a layer of impurities with concentration c, the transport along the y-axis can be determined from the average perturbed Keldysh Green's function, $\langle\hat{\mathbb{G}}^<\rangle$, which can be determined by integrating over $\overrightarrow{\rho}$ (namely integrating over the in-plane unit area $\square$) and multiplying by the concentration c of impurities [31,32]. More specifically, the *average* net $\langle T_\parallel\rangle$ and $\langle T_\perp\rangle$ on the right FM lead can be determined from[31]

$$\langle T_{\parallel(\perp)}\rangle = \frac{et}{16\pi^3\hbar}\int Tr[(\langle\hat{\mathbb{G}}^<_{\alpha' b}\rangle - \langle\hat{\mathbb{G}}^<_{b\alpha'}\rangle)\sigma_{x(y)}]dEd\mathbf{k}_\parallel, \quad (3)$$

where α' is the first site of the right FM lead, b is the last site in the IB, σ= $(\sigma_x, \sigma_y, \sigma_z)$ is the vector of the 2x2 Pauli matrix and $\mathbf{k}$ is the transverse component of the wave vector. For the case of two impurity layers at the left $l = a$ and right $l = b$ FM/IB interfaces, the $\langle T_\parallel\rangle$ and $\langle T_\perp\rangle$ are simply the sum of the single a- and b-layer contribution. A more appropriate treatment of the

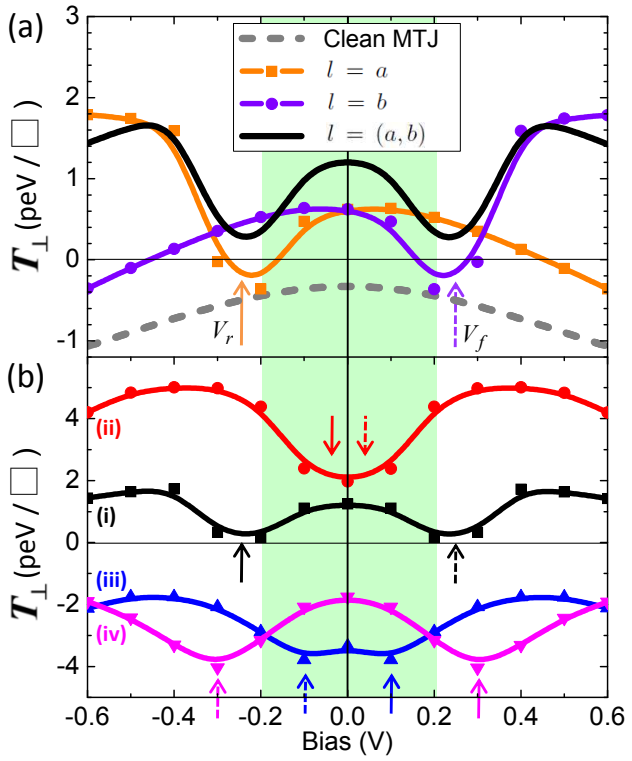

FIG. 2: (Color online) (a) Bias behavior of $T_\perp(\theta = \pi/2)$ per unit interfacial area, □, for the clean MTJ, and of $\langle T_\perp(\theta = \pi/2)\rangle$ for a single impurity layer at the left ($l = a$) and right interface ($l = b$), and for two impurity layers at both interfaces, ($l = a, b$), with ε_{imp}=0 eV. (b) Bias behavior of $\langle T_\perp(\theta = \pi/2)\rangle$ for the two impurity layers $l = (a, b)$ with ε_{imp} = (i) 0 eV, (ii) 0.2eV, (iii) 0.4eV, and (iv) 0.6 eV, respectively. The dashed and solid arrows, V_f and V_r, denote the critical forward and reverse bias at which the interfacial impurity resonances enter the bias window where $\langle T_\perp(V)\rangle$ reaches its minimum. The green shaded area denotes the low-bias region.

disorder is the coherent potential approximation (CPA) approach for the alloy, rather the simpler approach we employed of a system of noninteracting impurities.

III. RESULTS AND DISCUSSION

In Figs. 1(a) and (b) we show schematically the two cases of disorder, where a single layer of non-magnetic impurities with on-site ε_{imp}=0 is at (a) the first IB layer ($l = a$) at the left FM/IB interface under -0.25V bias and (b) the last IB layer ($l = b$) at the right IB/FM interface under +0.25V bias, respectively. The magnetization of the right, $\mathbf{M_R}$, and left, $\mathbf{M_L}$, semi-infinite FM leads sandwiching the IB, are along the z and x directions, respectively, with the y direction normal to the FM/B interface. Under a rotation operation of $\mathbf{M_L}$ along the direction of $\mathbf{M_R}$ the majority- (minority-) energy bands of the left lead acquire an additional minority- (majority-) energy band contribution, shown with the blue (red) arrows in the left lead in Figs. 1(a) and (b) . The magenta and cyan solid circles denote the impurity-induced resonance energies, E_1 and E_2, of the $\hat{\mathbb{T}}$-matrices in Eq. (1), respectively. The bias dependence of E_1 and E_2 for the two cases of disorder are plotted in Figs. 1(c) and (d), respectively, where μ_L is fixed at the Fermi energy, E_F =0 eV, $\mu_R = eV$ varies linearly with bias, and the green shaded area denotes the energy window between μ_L and μ_R. For $l = a$ both E_1 and E_2 are independent of V, because the impurity layer is at the left interface where $\mu_L = E_F$. In sharp contrast, both E_1 and E_2 vary linearly with V when the impurity layer is at the right interface, following the bias dependence of μ_R.

In Fig. 2(a) we compare the bias behavior of $T_\perp(\theta = \pi/2)$ for the clean MTJ with the *average* $\langle T_\perp(\theta = \pi/2)\rangle$ for disordered (ε_{imp}= 0) MTJs with a single impurity layer at the left ($l = a$) or right ($l = b$) interface and two impurity layers ($l = a, b$) at both interfaces. A single impurity layer at the left (right) interface changes the purely quadratic bias behavior of the clean MTJ to an asymmetric one, exhibiting a dip at $\sim V_r$=-0.25V (V_f=+0.25V) and a sign reversal in the negative (positive) bias regime. This is due to the fact that the impurity-induced resonance energies, E_1 and E_2, enter the bias window when $V < -0.25V$ ($V > +0.25V$) [Figs. 1(c) and (d)], thus enhancing the average field-like spin torque. On the other hand, in the positive (negative) bias region, where both E_1 and E_2 lie outside the bias window, $\langle T_\perp(V)\rangle$ exhibits a nearly quadratic bias behavior similar to that of the clean MTJ.

We have demonstrated that the asymmetry in the bias behavior of $T_\perp(V)$ can be controlled by changing the band filling or the energy barrier between two FM leads[14]. Thus, the asymmetric bias behavior of $\langle T_\perp\rangle$ in Fig. 2(a) arises from the impurity-induced resonance energies which in turn modify the barrier heights for the two FM leads. Furthermore, $\langle T_\perp(l = a, V < 0)\rangle \simeq \langle T_\perp(l = b, V > 0)\rangle$ ($\langle T_\perp(l = a, V > 0)\rangle \simeq \langle T_\perp(l = b, V < 0)\rangle$) due to the fact that the impurity-modified barrier heights for the left (right) FM lead for $l = a$ ($l = b$) is equal to that for the right (left) FM lead for $l = b$ ($l = a$). In sharp contrast, the two impurity layers at both the left and right FM/IB interfaces render the MTJ and the bias behavior of $\langle T_\perp(l = a, b)\rangle = \langle \sum_l T_\perp(l)\rangle$ symmetric. In addition, $\langle T_\perp\rangle$ exhibits a sinusoidal angular behavior for all asymmetric and symmetric disordered MTJs, similar to that of the clean junctions.

In Fig. 2(b) we display the bias behavior of $\langle T_\perp(\theta = \pi/2)\rangle$ for the case of a symmetric ($l = a, b$) disordered MTJ for various values of ε_{imp}. The dashed (solid) arrows, V_f (V_r), denote the critical forward (reverse) bias at which E_1 and E_2 of the single impurity interface layer enter the bias window where the spin torque reaches its minimum. The linear variations of E_1 and E_2 with ε_{imp}, i.e. $E_1 = -0.3eV + 0.9\varepsilon_{imp}$ and $E_2 = -0.2eV + 1.1\varepsilon_{imp}$, give rise to a shift of both critical biases which in turn have a dramatic effect on the bias behavior of $\langle T_\perp\rangle$. The

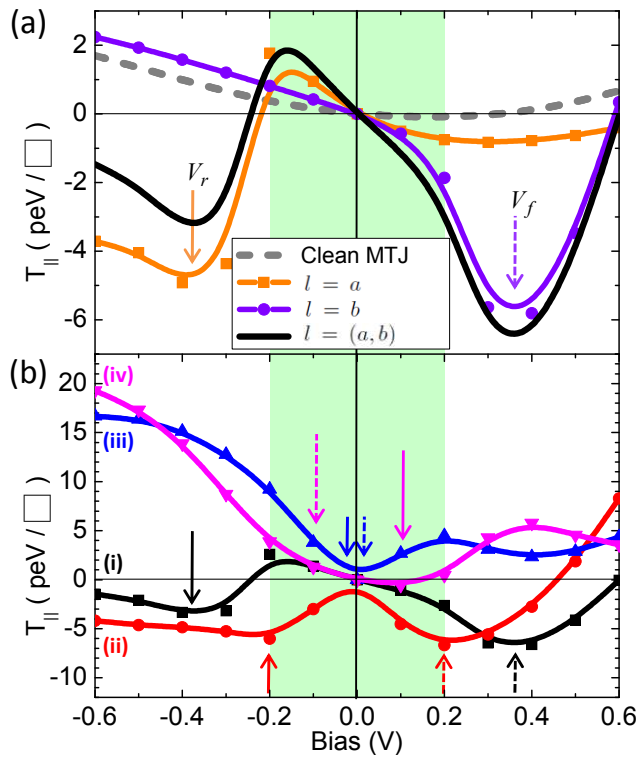

FIG. 3: (Color online) (a) Bias dependence of $T_{\|}(\theta = \pi/2)$ for the clean MTJ and of $\langle T_{\|}(\theta = \pi/2)\rangle$ for the disordered (ε_{imp}=0 eV) MTJ with a single impurity layer at the left ($l = a$) or right ($l = b$) interface and with two symmetric left and right interface impurity layers, ($l = a, b$), respectively. (b) Bias behavior of $\langle T_{\|}(\theta = \pi/2)\rangle$ for the symmetric disordered MTJ with ε_{imp} = (i) 0 eV, (ii) 0.2eV, (iii) 0.4eV, and (iv) 0.6eV, respectively. The dashed and solid arrows, V_f and V_r, represent the forward and reverse bias at which the interfacial impurity resonances enter the bias window where $\langle T_{\perp}(V)\rangle$ reaches its minimum. The green shaded area denotes the low-bias region.

most striking feature in Fig. 2(b) is the low-bias (shaded green region) behavior of $\langle T_{\perp}\rangle$ which can change from purely quadratic with positive or negative curvature to an almost bias-independent behavior. More importantly, the symmetric interfacial disorder not only gives rise to an enhancement of $\langle T_{\perp}\rangle$ compared to that in clean MTJs, but it can also lead to the sign reversal of $\langle T_{\perp}\rangle$ with ε_{imp}. These intriguing alloying effects offer an important external electronic handle through which the bias behavior of the average IEC can be exploited in future CIMR applications.

In Fig. 3(a) we show the bias dependence of the spin-transfer component, $T_{\|}(\theta = \pi/2)$, for the clean MTJ and compare it with the *average* $\langle T_{\|}(\theta = \pi/2)\rangle$ for the disordered (ε_{imp}= 0) MTJs with a single impurity layer at the left ($l = a$) or right ($l = b$) FM/IB interface and with two symmetric interfacial impurity layers ($l = a, b$), respectively. As in the case of $\langle T_{\perp}\rangle$, for the single impurity layer at the left (right) interface there is a significant change of $\langle T_{\|}\rangle$ in the negative (positive) bias range, where the spin-transfer component exhibits a non-monotonic behavior reaching its minimum at -0.35V (+0.35V) and a two-order enhancement compared to its value for the clean MTJ. On the other hand, the bias behavior in the positive (negative) window remains similar to that for the clean junction. This is due to the impurity-induced resonance energies entering the bias window, thus enhancing the transmission of the left (right) flowing electrons shown in Fig. 1(a) and (b). In Fig. 3(b) we present the bias dependence of $\langle T_{\|}(\theta = \pi/2)\rangle$ for the symmetric ($l = a, b$) disordered MTJ for various values of ε_{imp}. As in the case of $\langle T_{\perp}\rangle$, the shift of the resonance energies via alloying leads to a dramatic variation of the low-bias behavior of $\langle T_{\|}\rangle$ from linear to quadratic.

Moreover, we have demonstrated that the general expression of the bias behavior of $\langle T_{\|}\rangle$ [Eq. (1) in[31]] remains valid even in the presence of disorder, but where all quantities are replaced with their average values. Thus, $\langle T_{\|}\rangle$ is directly related to the spin current densities in collinear configurations, which can in turn lead to the enhancement of $\langle T_{\|}\rangle$. On the other hand, $\langle T_{\perp}\rangle$ is related to the interplay between the four non-equilibrium interlayer exchange couplings in collinear configurations[14].

Our calculations demonstrate that for our parameter set, when $0 \leq \varepsilon_{imp} - E_F \leq 0.6$ eV, and the impurity-induced resonance energies lie outside the bias window, both $\langle T_{\|}\rangle$ and $\langle T_{\perp}\rangle$ for symmetric ($l = a, b$) disordered junctions exhibit a low-bias ($|V| \leq 0.2$V) behavior similar to that of the clean MTJs, and agree qualitatively with the experimental measurements in the low-bias region [11–13]. The formation of a B oxide and the reduction of the Fe (Co) oxide at the interface reported in recent x-ray photoelectron spectroscopy [20] and three-dimensional atom probe studies [21], is similar to our case of symmetric ($l = a, b$) disordered MTJs. However the crystal structure of the Mg-B-O region remains unknown and where the boron resides after sputtering and subsequent annealing has remained a mystery. Recent *ab initio* calculations of the ordered magnesium borate ($Mg_2B_2O_5$) in its monoclinic and triclinic structure indicate that the sharp peaks at the bottom of the conduction band are due to B/p states [33]. However, the position of the B-impurity energies in the actual FeCoB/MgO/FeCoB MTJs remains unresolved. Thus, the current studies of the effect of disorder on the bias behavior of both components of spin torque where the on-site energy of the impurity is treated as a parameter may serve as simple guiding rules for future experimental studies.

IV. CONCLUSION

In conclusion, we presented for the first time calculations of the crucial effect of asymmetric and symmetric interfacial disorder on the bias behavior of the spin-transfer and field-like components of the spin torque. We have demonstrated that this can lead to strong enhance-

ment, sign reversal, and bias asymmetry, and have elucidated that the underlying electronic mechanism is the impurity-induced resonance energies. These findings may motivate further experimental studies of the crucial alloying effect so as to tune the bias behavior of both spin torque components and hence optimize the CIMS.

This work was supported by the NSF-PREM Grant Nos. DMR-0611562 and DMR-0958596, and the National Science Council of Taiwan under Contract No. NSC 99-2112-M-008-020-MY3.

* E-mail at:yhtang@cc.ncu.edu.tw.
† E-mail at:nick.kioussis@csun.edu.

[1] S. Parkin, J. Xin, C. Kaiser, A. Panchula, K. Roche, and M. Samant, Proceedings of the IEEE **91**, 661 (2003).
[2] S. I. Kiselev, J. C. Sankey, I. N. Krivorotov, N. C. Emley, R. J. Schoelkopf, R. A. Buhrman, and D. C. Ralph, Nature **425**, 380 (2003).
[3] S. Kaka, M. R. Pufall, W. H. Rippard, T. J. Silva, S. E. Russek, and J. A. Katine, Nature **437**, 389 (2005).
[4] C. Chappert, A. Fert, and F. N. V. Dau, Nat. Matter. **6**, 813 (2007).
[5] Y. Huai, F. Albert, P. Nguyen, M. Pakala, and T. Valet, Appl. Phys. Lett. **84**, 3118 (2004).
[6] G. D. Fuchs, N. C. Emley, I. N. Krivorotov, P. M. Braganca, E. M. Ryan, S. I. Kiselev, J. C. Sankey, D. C. Ralph, R. A. Buhrman, and J. A. Katine, Appl. Phys. Lett. **85**, 1205 (2004).
[7] J. C. Slonczewski, Phys. Rev. B **39**, 6995 (1989).
[8] L. Berger, Phys. Rev. B **54**, 9353 (1996).
[9] I. Theodonis, N. Kioussis, A. Kalitsov, M. Chshiev, and W. H. Butler, Phys. Rev. Lett. **97**, 237205 (2006).
[10] A. Kalitsov, M. Chshiev, I. Theodonis, N. Kioussis, and W. H. Butler, Phys. Rev. B **79**, 174416 (2009).
[11] H. Kubota, A. Fukushima, K. Yakushiji, T. Nagahama, S. Yuasa, K. Ando, H. Maehara, Y. Nagamine, K. Tsunekawa, D. D. Djayaprawira, N. Watanabe, and Y. Suzuki, Nature Phys. **4**, 37 (2008).
[12] J. C. Sankey, Y. -T. Cui, J. Z. Sun, J. C. Slonczewski, R. A. Buhrman, and D. C. Ralph, Nature Phys. **4**, 67 (2008).
[13] C. Wang, Y.-T. Cui, J. A. Katine, R. A. Buhrman, and D. C. Ralph, Nature Phys. **7**, 496 (2011).
[14] Y. -H. Tang, N. Kioussis, A. Kalitsov, W. H. Butler, and R. Car, Phys. Rev. Lett. **103**, 057206 (2009).
[15] Y. -H. Tang, N. Kioussis, A. Kalitsov, W. H. Butler, and R. Car, Phys. Rev. B **81**, 054437 (2010).
[16] S. -C. Oh, S. -Y. Park, A. Manchon, M. Chshiev, J. -H. Han, H. -W. Lee, J. -E. Lee, K. -T. Nam, Y. Jo, Y. -C. Kong, B. Dieny, and K. -J. Lee, Nature Phys. **5**, 898 (2009).
[17] S. S. P. Parkin, C. Kaiser, A. Panchula, P. M. Rice, B. Hughes, M. Samant, and S. -H. Yang, Nat. Mater. **3**, 862 (2004).
[18] S. Yuasa, T. Nagahama, A. Fukushima, Y. Suzuki, and K. Ando, Nat. Mater. **3**, 868 (2004).
[19] P. G. Mather, J. C. Read, and R. A. Buhrman, Phys. Rev. B **73**, 205412 (2006).
[20] J. C. Reed, P. G. Mather, and R. A. Buhrman, Appl. Phys. Lett. **90**, 132503 (2007).
[21] S. Pinitsoontorn, A. Cerezo, A. K. Petford-Long, D. Mauri, L. Folks, and M. J. Carey, Appl. Phys. Lett. **93**, 071901 (2008).
[22] J. P. Velev, K. D. Belashchenko, S. S. Jaswal, and E. Y. Tsymbal, Appl. Phys. Lett. **90**, 072502 (2007).
[23] Y. Ke, K. Xia, and H. Guo, Phys. Rev. Lett. **105**, 236801 (2010).
[24] M. Ye. Zhuravlev, E. Y. Tsymbal, and A. V. Vedyayev, Phys. Rev. Lett. **94**, 026806 (2005).
[25] S. Ikeda, J. Hayakawa, Y. Ashizawa, Y. M. Lee, K. Miura, H. Hasegawa, M. Tsunoda, F. Matsukura, and H. Ohno, Appl. Phys. Lett. **93**, 082508 (2008).
[26] W. H. Butler, X. -G. Zhang, T. C. Schulthess, and J. M. MacLaren, Phys. Rev. B **63**, 054416 (2001).
[27] J. Mathon and A. Umerski, Phys. Rev. B **63**, 220403 (R) (2001).
[28] J. D. Burton, S. S. Jaswal, E. Y. Tsymbal, O. N. Mryasov, and O. G. Heinonen, Appl. Phys. Lett. **89**, 142507 (2006).
[29] A. Manchon, N. Ryzhanova, N. Strelkov, A. Vedyayev, and B. Dieny, J. Phys.: Condens. Matter **19**, 165212 (2007).
[30] T. Birol and P. W. Brouwer, Phys. Rev. B. **80**, 014434 (2009).
[31] Y. -H. Tang, N. Kioussis, A. Kalitsov, and R. Car, J. Appl. Phys. **109**, 07C920 (2011).
[32] A. Kalitsov, A. Coho, N. Kioussis, A. Vedyayev, M. Chshiev and A. Granovsky, Phys. Rev. Lett. **93**, 046603 (2004).
[33] Derek A. Stewart, Nano Lett. **10**, 263 (2010).